A strong regioregularity effect in self-organizing conjugated polymer films and high-efficiency polythiophene:fullerene solar cells

YOUNGKYOO KIM[1]*, STEFFAN COOK[2], SACHETAN M. TULADHAR[1], STELIOS A. CHOULIS[1], JENNY NELSON[1]*, JAMES R. DURRANT[2], DONAL D. C. BRADLEY[1]*, MARK GILES[3], IAIN MCCULLOCH[3], CHANG-SIK HA[4] AND MOONHOR REE[5]

[1]Department of Physics, Blackett Laboratory, Imperial College London, London SW7 2BW, UK
[2]Department of Chemistry, Imperial College London, London SW7 2AZ, UK
[3]Merck Chemicals, Chilworth Science Park, Southampton SO16 7QD, UK
[4]Department of Polymer Science and Engineering, Pusan National University, Pusan 609-735, South Korea
[5]Department of Chemistry & Pohang Accelerator Laboratory, Pohang University of Science and Technology, Pohang 790-784, South Korea
*e-mail: y.kim@ic.ac.uk; jenny.nelson@imperial.ac.uk; d.bradley@imperial.ac.uk

Published online: 5 February 2006; doi:10.1038/nmat1574

Low-cost photovoltaic energy conversion using conjugated molecular materials has become increasingly feasible through the development of organic 'bulk heterojunction (BHJ)' structures[1–7], where efficient light-induced charge separation is enabled by a large-area donor–acceptor interface[2,3]. The highest efficiencies have been achieved using blends of poly(3-hexylthiophene) (P3HT) and a fullerene derivative[8–12], but performance depends critically on the material properties and processing conditions. This variability is believed to be influenced by the self-organizing properties of P3HT, which means that both optical[13,14] and electronic[15,16] properties are sensitive to the molecular packing. However, the relationship between molecular nanostructure, optoelectronic properties of the blend material and device performance has not yet been demonstrated. Here we focus on the influence of polymer regioregularity (RR) on the molecular nanostructure, and hence on the resulting material properties and device performance. We find a strong influence of RR on solar-cell performance, which can be attributed to enhanced optical absorption and transport resulting from the organization of P3HT chains and domains. Further optimization of devices using the highest RR material resulted in a power conversion efficiency of 4.4%, even without optimization of electrodes[7].

Polymer/fullerene BHJ solar cells have a layered structure (Fig. 1a) in which the light is incident on the BHJ layer, here blend films of P3HT and 1-(3-methoxycarbonyl)-propyl-1-phenyl-(6,6) C_{61} (PCBM), through the indium/tin-oxide (ITO)-coated glass substrate[6,10]. Light absorption by this BHJ layer generates excitons that are dissociated into holes and electrons by charge separation between the electron-donor (P3HT) and the electron-acceptor (PCBM)[10]. Photocurrent generation by devices based on such blends is limited by the poor red-light absorption of the polymer and the low mobilities for charge transport to the electrodes[5]. Both the optical[13] and transport[15] properties of pristine P3HT polymer films are known to improve with the degree of RR, defined as the percentage of monomers adopting a head-to-tail configuration rather than head-to-head (Fig. 1). RR P3HT chains tend to stack into planar structures known as 'lamellae', which are normally oriented perpendicular to the substrate (see the schematic for lamella folding in Fig. 1b). Higher RR enables closer packing of these lamellae such that the optical[13] and charged[17] excitations adopt some interchain character. These interchain contributions are believed to be responsible for the distinct shoulder observed on the long-wavelength side of the absorption maximum[13] and for the larger field-effect mobility[15] in high RR P3HT films. In Fig. 1b we illustrate the influence of RR on chain packing using an energy-minimized molecular structure of 11 units of P3HT with RR of 100% and 90%. Even though the interchain spacing within the thiophene ring plane (d_{a-a}) (herein referred to as intraplane stacking) is found to be unaffected by this variation in RR, the interchain spacing perpendicular to the ring plane (d_{b-b}) (referred to as interplane stacking) is found to increase in the lower RR case, indicating that higher RR should indeed increase interchain interactions. Moreover, the tendency of lamellae to orient normal to the substrate in ordered films has been suggested to increase optical anisotropy leading to higher absorption for

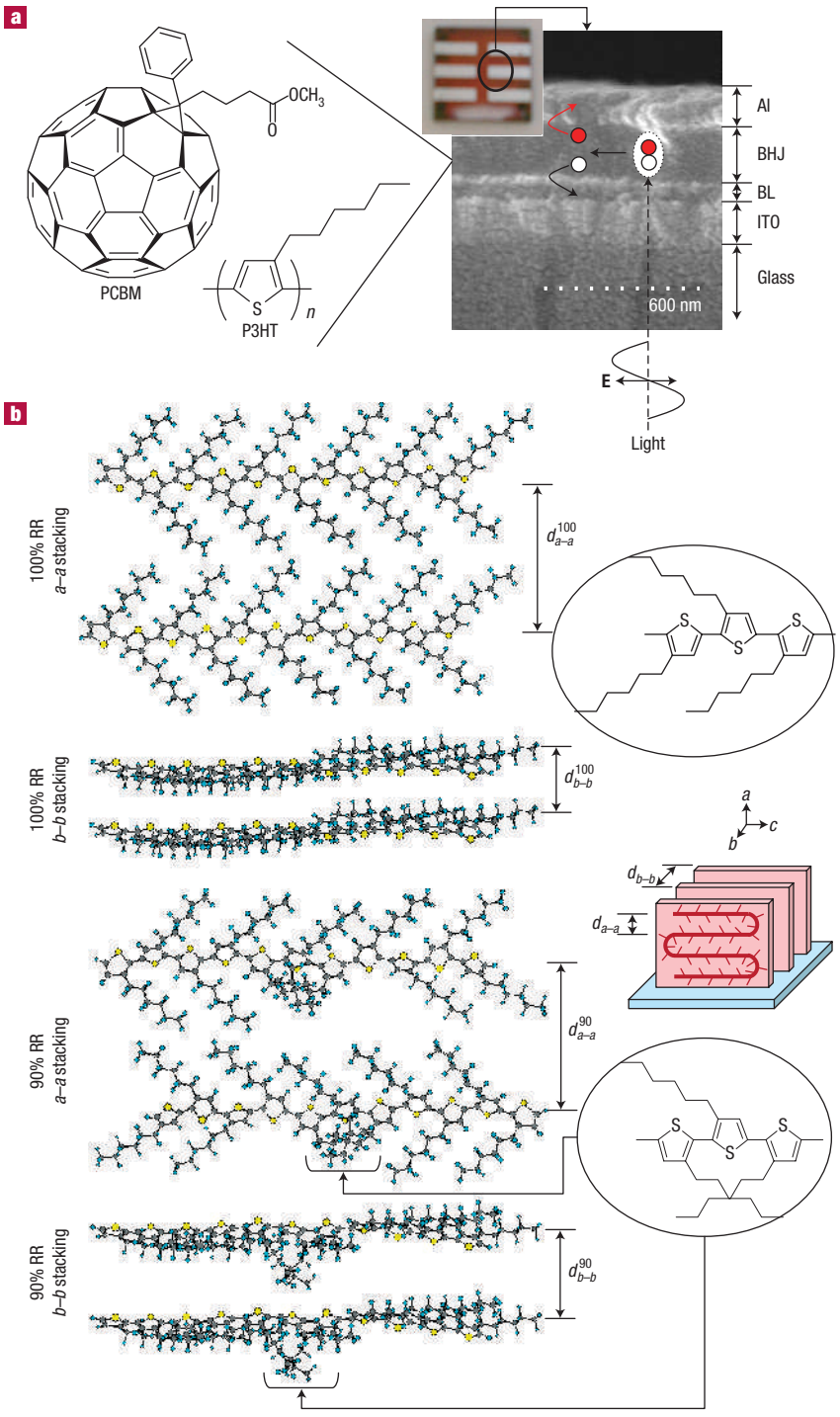

Figure 1 Schematic structure of polymer solar cells and energy-minimized structure of P3HTs. a, Cross-sectional structure (SEM, main image) of a polymer solar cell (inset photograph: top-view) with a BHJ layer (P3HT + PCBM) and a PEDOT:PSS layer (BL). The exciton generation and charge (electrons in red circles; holes in white circles) separation/collection under depolarized light illumination (**E** is the electric field vector) are shown schematically. **b**, The energy-minimized molecular structure of P3HTs (11 repeating units per chain) for 100% RR (d^{100}_{a-a} and d^{100}_{b-b} are the *a*-direction and *b*-direction chain-stacking spacings, respectively) and 90% RR (d^{90}_{a-a} and d^{90}_{b-b} are the corresponding spacings). The *a*-direction and *b*-direction are parallel and perpendicular to the thiophene ring plane, respectively (see the chemical structures within the ovals as well as the schematic illustration for lamella folding and ordering on a substrate).

light incident normal to the substrate[14]. Achieving similar ordering of P3HT chains within a BHJ structure is therefore desirable, as it promises higher optical absorption and improved transport properties, although in a BHJ the segregation of donor and acceptor phases must also be considered. Despite the recognized importance of RR in influencing chain packing and ordering,

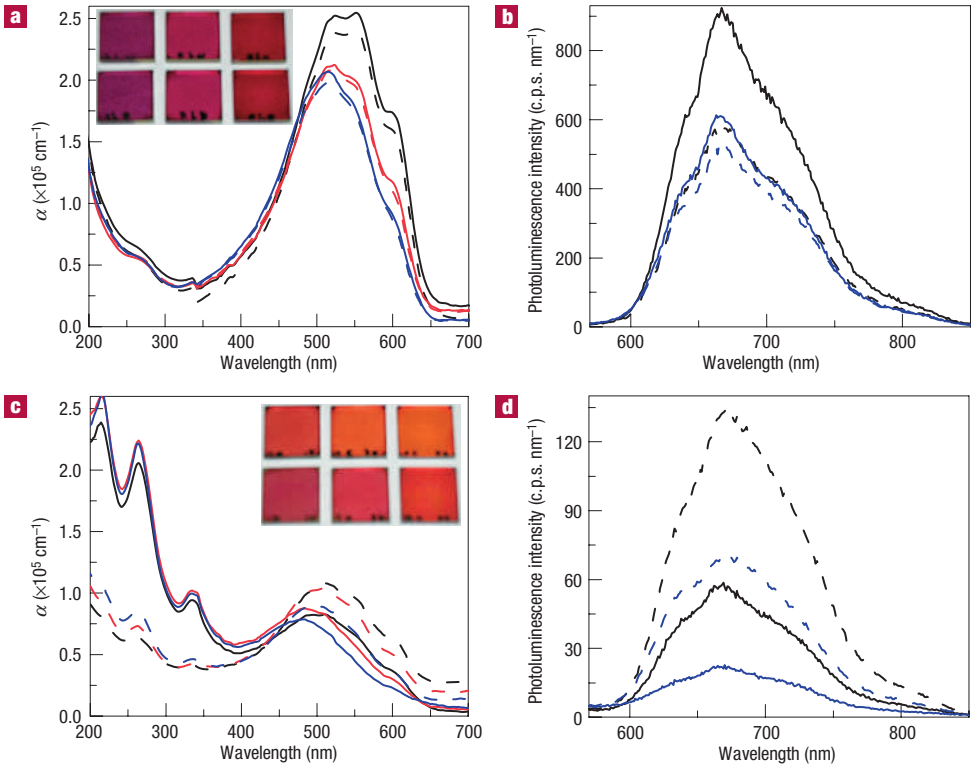

Figure 2 Optical spectra of pristine and blend films. a–d, Optical absorption and photoluminescence spectra (93% RR omitted) of pristine P3HT films (**a**,**b**, approximately 100 nm thick) and P3HT:PCBM (1:1) blend films (**c**,**d**, approximately 200 nm thick): black, red and blue colours represent 95.2%, 93% and 90.7% RR, respectively, and solid and dashed lines denote not-annealed and annealed (140 °C for 2 h) films, respectively. c.p.s. is counts per second. Insets to **a**,**c**: photographs of films, sample size 12 mm × 12 mm; from left 95.2%, 93% and 90.7% RR; top, not-annealed; bottom, annealed.

its influence on the performance of BHJ solar cells has not yet been demonstrated.

In this work we demonstrate that the performance of P3HT:PCBM solar cells is improved by both increasing RR and annealing, and that these improvements result from the beneficial impact of P3HT chain packing on the optical and transport properties of the blend. The effect of chain stacking on the optical properties of pristine and blend films made from P3HTs with three different degrees of RR is illustrated in Fig. 2. For pristine P3HT films, the absorption coefficient α increases with increasing RR, particularly on the red shoulder at 600 nm, which is assigned to interplane interactions[13] (see the colour changes on the photographs in Fig. 2a). No striking absorption coefficient changes result, however, from thermal annealing at 140 °C. From the intensity of photoluminescence spectra of the pristine P3HT (Fig. 2b) it is clear that higher RR tends to increase photoluminescence intensity, suggesting a reduction in non-radiative quenching pathways in the more ordered material. Annealing of the highest RR films invokes a slight reduction in photoluminescence intensity. For the P3HT:PCBM (1:1) blend films, the absorption coefficient trends are the same as for the pristine films with respect to RR, with a growth in the red shoulder attributed to interplane interactions, showing that self-organization of P3HT is still effective even in the presence of 50 wt% PCBM (Fig. 2c)[10]. After thermal annealing, all blend films show increased absorption coefficient and photoluminescence intensity (Fig. 2d)[10]. These effects are attributed to the segregation of ordered P3HT domains, with improved intraplane and interplane stacking, out of the blend on thermal annealing.

The influence of RR and annealing on intraplane chain stacking in the pristine and blend films is demonstrated with grazing-incidence X-ray-diffraction (GIXRD) measurements using a synchrotron X-ray beam (Fig. 3a). As shown in Fig. 3c (Fig. 3b for two-dimensional images), the out-of-plane (OOP) diffraction patterns (diffraction angle $2\theta = 5.3°$, $10.7°$ and $15.9°$ for the primary (100), secondary (200) and tertiary (300) peaks) indicate that all pristine P3HT films show a well-organized intraplane structure with lamellae oriented normal to the substrate (see the schematic for lamella folding in Fig. 1b)[15], with the degree of order, inferred from the peak intensity, increasing with RR. From the in-plane (IP) patterns (inset to Fig. 3c) the RR effect is clearly observed: the higher RR, the weaker the intraplane stacking in the plane of the substrate, indicating that intraplane stacking perpendicular to the substrate is most pronounced[15]. After thermal annealing, this contrast in the peak intensity for OOP and IP geometries becomes more pronounced, whilst the trend with RR is preserved. For the blend film with the 90.7% RR P3HT, the primary peak in both OOP and IP geometries is greatly reduced compared with the pristine polymer, indicating that intraplane stacking almost disappears on blending with PCBM molecules, whereas the blend films with higher RR P3HTs still show the intraplane stacking features. After thermal annealing, this intraplane stacking feature is enhanced for all the blend films, showing clear primary and secondary peaks in both OOP and IP geometries. This indicates an increase in the size or number of P3HT crystallites in the blend films on thermal annealing, supporting the increased photoluminescence intensity on annealing (see Fig. 2d). Therefore, these GIXRD results support the proposal that the thermal

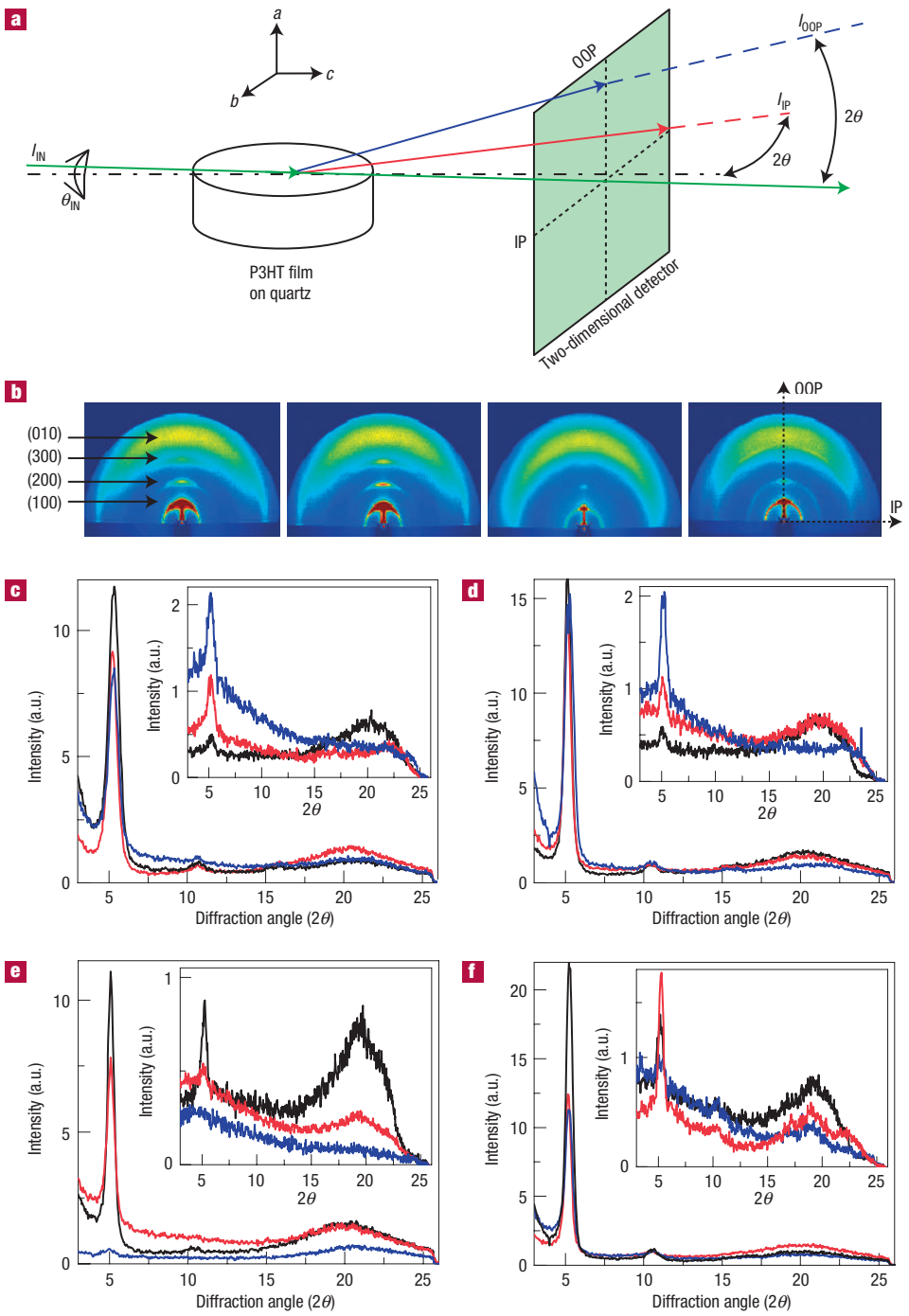

Figure 3 GIXRD setup and results for pristine and blend films. a,**b**, Schematic illustration (**a**) of the two-dimensional GIXRD measurement (incident X-ray angle $\theta_{IN} = 0.2^{\circ}$) and representative two-dimensional images (**b**) of pristine P3HT film (not-annealed in first from left; annealed in second from left) and P3HT:PCBM (1:1) blend films (not-annealed in third from left; annealed in fourth from left). I_{IN}, incident X-ray intensity; I_{OOP}, diffracted X-ray intensity in the OOP direction; I_{IP}, diffracted X-ray intensity in the IP direction. **c**–**f**, OOP GIXRD diffractograms of pristine P3HT films (**c**, not-annealed; **d**, annealed) and P3HT:PCBM (1:1) blend films (**e**, not-annealed; **f**, annealed; approximately 200 nm thick): insets show corresponding IP GIXRD patterns. Black, red and blue colours represent 95.2%, 93% and 90.7% RR, respectively.

annealing of blend films at 140 °C strongly develops the intraplane chain stacking perpendicular to the film substrate and, in the case of low RR polymers, stimulates the segregation of crystalline P3HT domains out of the disordered blend.

The influence of these differences in chain packing with RR is examined for polymer solar cells made with the blend films. The devices have the layer structure shown in Fig. 1a with a blend film thickness of ~200 nm. A comparison of current-density–voltage (J–V) characteristics under air-mass 1.5 simulated irradiance shows that the short-circuit current density (J_{SC}) and external quantum efficiency (EQE) (Fig. 4a,b) both increase with the RR of P3HT. This is attributed partly to the enhanced red-light

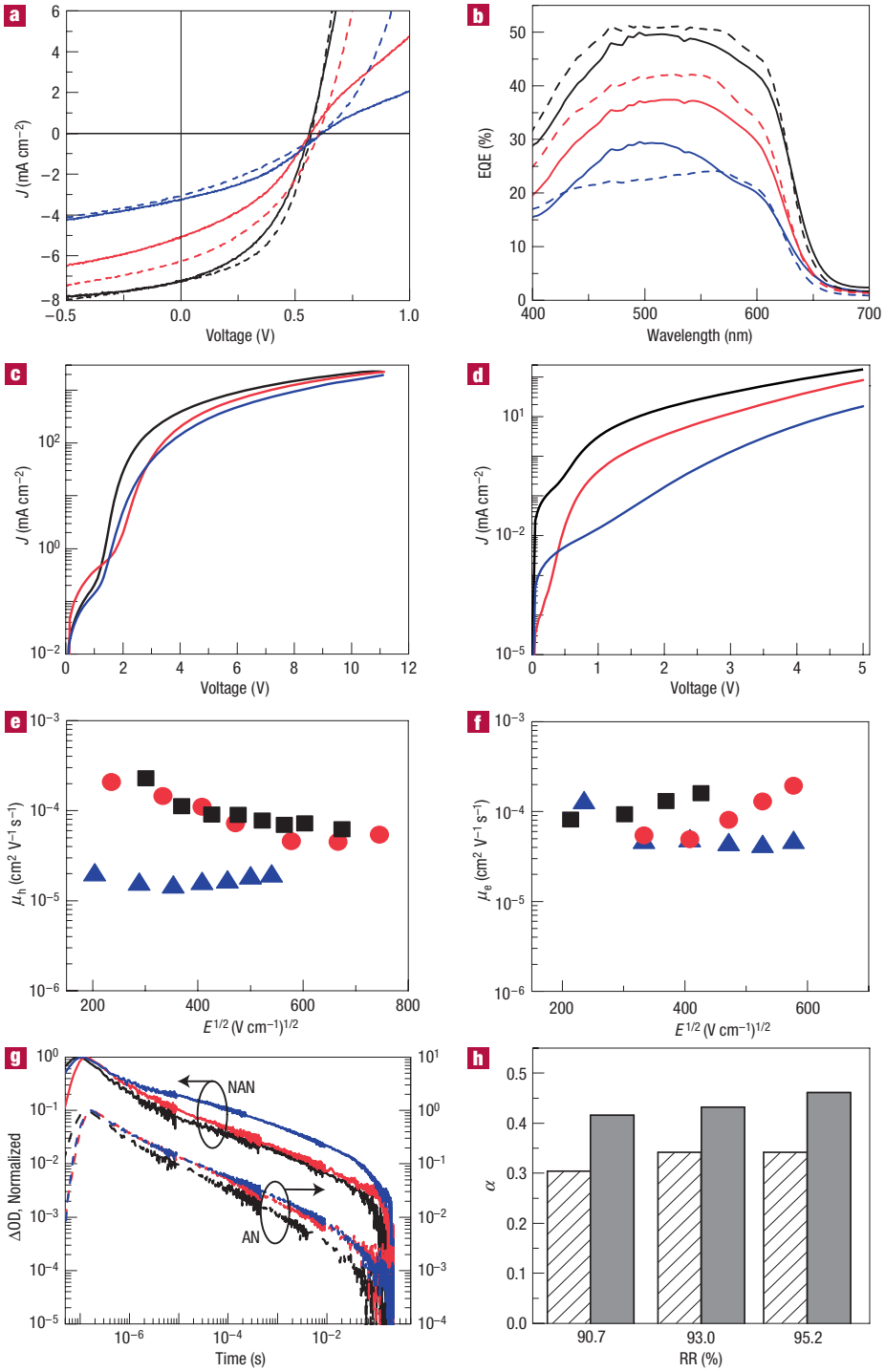

Figure 4 Electrical properties and polaron dynamics of pristine and/or blend films. a,**b**, Light *J*–*V* characteristics (air mass 1.5, incident-light power density $P_{IN} = 85$ mW cm^{-2}) (**a**) and EQE spectra (**b**) of the devices with P3HT:PCBM (1:1) blend films (approximately 200 nm thick): symbol and line colours are as in Fig. 2. Solar-cell characteristics are summarized as follows: for not-annealed device with 95.2% RR P3HT, $J_{SC} = 7.26$ mA cm^{-2}, open circuit voltage $V_{OC} = 0.56$ V, fill factor FF = 43.9%, PCE = 2.1%; for annealed device with 95.2% RR, $J_{SC} = 7.28$ mA cm^{-2}, $V_{OC} = 0.57$ V, FF = 49.7%, PCE = 2.4%; for not-annealed device with 93% RR, $J_{SC} = 5.1$ mA cm^{-2}, $V_{OC} = 0.57$ V, FF = 37.8%, PCE = 1.3%; for annealed device with 93% RR, $J_{SC} = 6.28$ mA cm^{-2}, $V_{OC} = 0.6$ V, FF = 39.4%, PCE = 1.8%; for not-annealed device with 90.7% RR, $J_{SC} = 3.27$ mA cm^{-2}, $V_{OC} = 0.62$ V, FF = 37.0%, PCE = 0.9%; for annealed device with 90.7% RR, $J_{SC} = 3.07$ mA cm^{-2}, $V_{OC} = 0.61$ V, FF = 32.1%, PCE = 0.7%. **c**,**d**, Dark *J*–*V* characteristics of not-annealed devices with pristine P3HT films (**c**) and P3HT:PCBM (1:1) blend films (**d**). **e**,**f**, Hole (**e**) and electron (**f**) mobilities (TOF) of P3HT:PCBM (1.2:1) blend films (approximately 1–2 μm thick) as a function of the square-rooted electric field ($E^{1/2}$): black squares, red circles and blue triangles, which were excited at 355 nm, denote the blend films prepared with 95.2%, 93% and 90.7% RR P3HT. **g**,**h**, Normalized ΔOD transients (**g**, line colours as in Fig. 2) of not-annealed (NAN) and annealed (AN) blend films (approximately 200 nm thick), and resulting slope (α) changes with respect to RR (**h**, hatched bar for not-annealed; grey bar for annealed blend films).

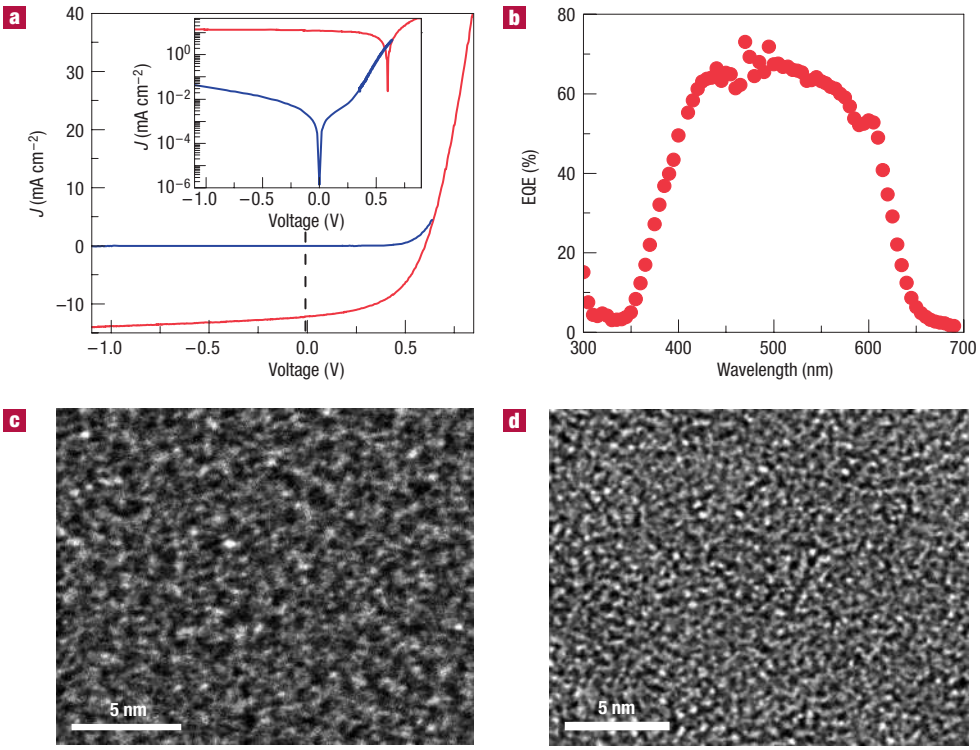

Figure 5 Best performance of polymer solar cells made in this work. a, Dark (blue line) and light (red line, air mass 1.5, $P_{IN} = 85$ mW cm^{-2}) *J–V* characteristics (inset with semi-logarithmic scale) of the annealed (140 °C for 2 h) device with P3HT:PCBM (1:1) blend films (approximately 175 nm thick). **b**, EQE spectrum ($P_{IN} = 33$ μW cm^{-2} at 520 nm) of the same device. **c**,**d**, FEG-TEM images of not-annealed (**c**) and annealed (**d**) blend films.

absorption by the higher RR P3HT owing to its more organized chain packing (see Fig. 1b). After thermal annealing, this trend was preserved. In addition, the fill factor was improved, partly owing to reduced series resistance, particularly for the devices with low RR P3HT. However, the effect of RR on absorption coefficient illustrated in Fig. 2c does not account for this large effect on J_{SC}: from the relative absorption coefficients of the 90.7% and 95.2% RR P3HT blend films, an increase in J_{SC} of only 10–20% can be expected on increasing RR from 90.7% to 95.2%, whilst the measured J_{SC} increases by more than 100% (see Supplementary Information). Therefore, the improvement in J_{SC} must arise from other factors such as improvement in charge transport with RR. For this reason, the charge-transport characteristics for blend films of different RR were investigated by measuring steady-state dark *J–V* characteristics and time-of-flight (TOF) mobilities[18].

The dark-current density of as-fabricated devices made with pristine P3HT increases with the RR of P3HT in the higher voltage regime (Fig. 4c). This trend is preserved after thermal annealing, and may be attributed to improved mobilities, improved injection or both. The increase in dark current is modest compared with the increases observed in field-effect hole mobility when regiorandom P3HT is replaced with high RR P3HT[15]. This may be expected because the preferred direction for interplane interchain (π–π) stacking, revealed by GIXRD measurements above, is parallel to the substrate, and the enhanced interplane interactions available with high RR are therefore less likely to benefit vertical (such as *J–V*) than lateral (such as field-effect) transport. TOF hole mobilities in thick (~1 μm) films of P3HT showed negligible influence of RR on either electron or hole mobility, again indicating that interplane stacking does not strongly affect vertical transport in the pristine polymer. In as-fabricated devices with blend films, the dark-current densities (Fig. 4d) and TOF mobilities (Fig. 4e,f) both show a stronger dependence on RR than for pristine films. The TOF hole mobility, μ_h, is about one order of magnitude lower for the blend film with 90.7% RR P3HT than for the higher RR P3HTs (Fig. 4e), which is consistent with the structural evidence for poor P3HT domain formation in that blend before annealing. The electron mobility, μ_e, also increases with RR, most probably owing to PCBM domain formation but possibly assisted by improved morphology for electron transport in the ambipolar P3HT[18]. From these *J–V* and TOF results we conclude that charge transport in blend films becomes faster with increasing RR of P3HT, and that the increase is correlated to improvements in P3HT chain packing and their influence on P3HT domain formation. The increased charge mobilities, together with the increase in light absorption, are capable of explaining the large increase in J_{SC} with RR.

Further evidence for this strong effect of RR on charge transport was obtained using transient absorption spectroscopy (TAS)[19,20], where the absorption ΔOD of photogenerated negative polarons[21] of PCBM in the blend films is monitored at 980 nm following low-intensity pulsed laser excitation (Fig. 4g). All blend films show a slow power-law decay, which is assigned to the diffusion-limited recombination of the remaining, separated charges. In the presence of deep traps for either charge, the slow decay dynamics reflect the detrapping of charges, which is the rate-limiting step for both recombination and charge transport. These dynamics are quantified by fitting the slow decay to a power law ($\Delta OD \sim t^{-\alpha}$), where t is time, $\alpha = T/T_0$, T is temperature and T_0 represents the characteristic temperature of an exponential distribution of charge traps. As shown in Fig. 4g, these decay dynamics are faster

(higher α) for the higher RR P3HT films (Fig. 4h), indicating fewer deep traps in the high RR blend films[19,20]. This is consistent with the faster hole transport in higher RR blend films demonstrated above. Annealed blend films show increased α regardless of RR, again indicating improved charge-carrier diffusion, which is ascribed to the improved ordering of P3HT chains on thermal annealing, as measured with GIXRD (see Fig. 3), and, moreover, indicating that some of the charge traps are of structural, rather than chemical, origin. Accordingly, these TAS results confirm that charge transport in these blend films is affected by the RR of P3HT as well as by thermal annealing, apparently through the effects of RR and thermal annealing on the self-organizing crystal structure of the P3HT.

On the basis of these results, we anticipate that the highest device efficiencies will be achieved with the highest RR P3HT. Previous studies show that thickness and annealing conditions influence device performance[10,22,23] and that they should be optimized for each batch of materials. Accordingly, we have achieved 4.4% power conversion efficiency (PCE) and 68–73% EQE (450–550 nm) using the P3HT polymer with the highest available RR (95.4%), after optimizing film thickness (~175 nm) and device annealing conditions (Fig. 5a,b). In particular, the optimized device showed very high dark rectification ratios of over 140 at ±0.6 V (open-circuit condition) and 2.1×10^3 at ±0.85 V (injection-limited regime), which indicates improved shunt and series resistances[24] by device annealing. This improved device performance is mainly ascribed to the enhanced film packing parallel to the substrate on thermal annealing as observed from the high-resolution transmission electron microscopy (TEM) images in Fig. 5c,d, which stress again the importance of interplane packing density.

METHODS

P3HTs with 90.7%, 93% and 95.2% RR were synthesized using the Merck synthetic method and were end-capped with hydrogen[25]. Weight (M_w) and number (M_n) average molecular weights, polydispersity indices (PDI), and melting points (T_m) were as follows: for 95.2% RR, $M_w = 2.19 \times 10^4$, $M_n = 1.42 \times 10^4$, PDI = 1.57, $T_m = 212$ °C; for 93% RR, $M_w = 3.19 \times 10^4$, $M_n = 1.78 \times 10^4$, PDI = 1.79, $T_m = 211$ °C; for 90.7% RR, $M_w = 4.59 \times 10^4$, $M_n = 2.37 \times 10^4$, PDI = 1.94, $T_m = 203$ °C (here we note that the trend in molecular weights is in the wrong direction to explain the present RR data). For the 4.4% PCE devices a separate batch of P3HT (95.4% RR), synthesized in the same way, was used: this was characterized by $M_w = 2.11 \times 10^4$, $M_n = 1.16 \times 10^4$, PDI = 1.82, $T_m = 222$ °C. All polymers were purified in the same manner to give typical metallic impurities Ni < 2 μg g^{-1} and Mg < 50 μg g^{-1}. PCBM was synthesized by the University of Groningen (The Netherlands) and used as received[26].

Pristine P3HT solutions were prepared using chlorobenzene (30 mg ml^{-1}). Blend solutions (P3HT:PCBM = 1:1 by weight)[10,22,23] for thin-film and device fabrication were prepared using chlorobenzene (60 mg ml^{-1}), whereas for TOF measurements concentrated blend solutions (P3HT:PCBM = 1.2:1 by weight) were prepared using chlorobenzene (120 mg ml^{-1}). For the characterization of film samples, the pristine and blend solutions were spin-coated onto quartz substrates (spectrosil B). It was found that the measured optical density of pristine P3HT films (~100 nm thick) was slightly higher or the same, whereas the thickness was increased by about 10–20% after thermal annealing. Polymer solar cells were fabricated in the same way as in ref. 10, and film and device annealing was carried out at 140 °C for 2 h inside a nitrogen-filled glove box[10]. The structures for TOF mobility measurements were fabricated in a similar way to those reported in refs 18,24.

The film and device measurements were performed as reported in previous studies, namely optical absorption as per ref. 24, solar-cell characteristics as per refs 10,24, TOF mobility as per refs 18,24 and photoluminescence measurements using an integrating sphere with excitation light at a wavelength $\lambda = 525$ nm as per ref. 24. For TAS measurements, the PCBM radical anion decay dynamics were obtained by pulsed excitation at 525 nm (repetition rate 4 Hz, pulse duration <1 ns, excitation density ~16 μJ cm^{-2}) monitoring the decay dynamics of the photoinduced absorption at 980 nm (0.8 eV) assigned primarily to PCBM radical anion absorption[19,21]. Scanning electron microscope (SEM) images were measured using an SEM/energy dispersive X-ray system (Hitachi S4200). Two-dimensional GIXRD images were measured using a high-power X-ray beam (photon flux ≈10^{11} photons s^{-1} $mrad^{-1}$ per 0.1%, beam size ≤0.5 mm^2) from a synchrotron radiation source (4C2 beamline, Pohang Accelerator Laboratory, South Korea) and a detection system equipped with a two-dimensional X-ray detector (PI-SCX4300-165/2, Princeton Instrument). The IP nanomorphology of blend films was measured using a high-resolution TEM equipped with a field emission gun (FEG-TEM, JEM-2100F, JEOL, Japan).

The energy-minimized molecular structures of 11 units of P3HT with RR of 100% and 90% were calculated using MM2 (CambridgeSoft).

Received 31 August 2005; accepted 1 December 2005; published 5 February 2006.

References

1. Tang, C. W. A two-layer organic solar cell. *Appl. Phys. Lett.* **48,** 183–185 (1986).
2. Sariciftci, N. S., Smilowitz, L., Heeger, A. J. & Wudl, F. Photoinduced electron transfer from a conducting polymer to buckminsterfullerene. *Science* **258,** 1474–1476 (1992).
3. Halls, J. J. M. *et al.* Efficient photodiodes from interpenetrating networks. *Nature* **376,** 498–500 (1995).
4. Yu, G., Gao, J., Hummelen, J. C., Wudl, F. & Heeger, A. J. Polymer photovoltaic cells: enhanced efficiencies via a network of internal donor-acceptor heterojunctions. *Science* **270,** 1789–1791 (1995).
5. Nelson, J. Organic photovoltaic films. *Mater. Today* **5,** 20–27 (2002).
6. Brabec, C. J., Sariciftci, N. S. & Hummelen, J. C. Plastic solar cells. *Adv. Funct. Mater.* **11,** 15–26 (2001).
7. Brabec, C. J., Shaheen, S. E., Winder, C., Sariciftci, N. S. & Denk, P. Effect of LiF/metal electrodes on the performance of plastic solar cells. *Appl. Phys. Lett.* **80,** 1288–1290 (2002).
8. Schilinsky, P., Waldauf, C. & Brabec, C. J. Recombination and loss analysis in polythiophene based bulk heterojunction photodetectors. *Appl. Phys. Lett.* **81,** 3885–3887 (2002).
9. Padinger, F., Ritterberger, R. S. & Sariciftci, N. S. Effects of postproduction treatment on plastic solar cells. *Adv. Funct. Mater.* **13,** 85–88 (2003).
10. Kim, Y. *et al.* Device annealing effect in organic solar cells with blends of regioregular poly(3-hexylthiophene) and soluble fullerene. *Appl. Phys. Lett.* **86,** 063502 (2005).
11. Reyes-Reyes, M., Kim, K. & Carroll, D. L. High-efficieny photovoltaic devices based on annealed poly(3-hexylthiophene) and 1-(3-methoxycarbonyl)-propyl-1-pheny-(6, 6)C_{61} blends. *Appl. Phys. Lett.* **87,** 083506 (2005).
12. Li, G. *et al.* High-efficiency solution processable polymer photovoltaic cells by self-organization of polymer blends. *Nature Mater.* **4,** 864–868 (2005).
13. Brown, P. J. *et al.* Effect of interchain interactions on the absorption and emission of poly(3-hexylthiophene). *Phys. Rev. B* **67,** 064203 (2003).
14. Zhokhavets, U., Gobsch, G., Hoppe, H. & Sariciftci, N. S. Anisotropic optical properties of thin poly(3-octylthiophene)-films as a function of preparation conditions. *Synth. Met.* **143,** 113–117 (2004).
15. Sirringhaus, H. *et al.* Two-dimensional charge transport in self-organized, high mobility conjugated polymers. *Nature* **401,** 685–688 (1999).
16. Kline, R. J. *et al.* Dependence of regioregular poly(3-hexylthiophene) film morphology and field-effect mobility on molecular weight. *Macromolecules* **38,** 3312–3319 (2005).
17. Österbacka, R., An, C. P., Jiang, X. M. & Vardeny, Z. V. Two-dimensional electronic excitations in self-assembled conjugated polymer nanocrystals. *Science* **287,** 839–842 (2000).
18. Choulis, S. A. *et al.* High ambipolar and balanced carrier mobility in regioregular poly(3-hexylthiophene). *Appl. Phys. Lett.* **85,** 3890–3892 (2004).
19. Montanari, I. *et al.* Transient optical studies of charge recombination dynamics in a polymer/fullerene composite at room temperature. *Appl. Phys. Lett.* **81,** 3001–3003 (2002).
20. Nelson, J. Diffusion-limited recombination in polymer-fullerene blends and its influence on photocurrent collection. *Phys. Rev. B* **67,** 155209 (2003).
21. Guldi, D. M., Hungerbühler, H. & Asmus, K.-D. Redox and excitation studies with C_{60}-substituted malonic acid diethyl esters. *J. Phys. Chem.* **99,** 9380–9385 (1995).
22. Kim, Y. *et al.* Composition and annealing effects in polythiophene/fullerene solar cells. *J. Mater. Sci.* **40,** 1371–1376 (2005).
23. Chirvase, D., Parisi, J., Hummelen, J. C. & Dyakonov, V. Influence of nanomorphology on the photovoltaic action of polymer-fullerene composites. *Nanotechnology* **15,** 1317–1323 (2004).
24. Kim, Y. *et al.* Organic photovoltaic devices based on blends of regioregular poly(3-hexylthiophene) and poly(9,9-dioctylfluorene-co-benzothiadiazole). *Chem. Mater.* **16,** 4812–4818 (2004).
25. Koller, G., Falk, B., Weller, C., Giles, M. & McCulloch, I. Process of preparing regioregular poly-(3-substituted) thiophenes. World patent WO2005/014691 (2005).
26. Hummelen, J. C. *et al.* Preparation and characterization of fulleroid and methanofullerene derivatives. *J. Org. Chem.* **60,** 532–538 (1995).

Acknowledgements

The authors thank Merck Chemicals for supplying the P3HT polymer and British Petroleum International for financial support through the OSCER project. Y.K. thanks G. Y. Heo (Postech, Korea), J. W. Park and H. J. Kim (PNU, Korea) for their help with the GIXRD and SEM measurements. Correspondence and requests for materials should be addressed to Y.K. or J.N. or D.D.C.B. Supplementary Information accompanies this paper on www.nature.com/naturematerials.

Competing financial interests

The authors declare that they have no competing financial interests.